Indian Journal of Pure & Applied Physics
Vol. 60, July 2022, pp. 590-599

Improved Photocatalytic Activity of Hydrothermally Prepared Bi_2WO_6 in Degradation of Rhodamine B and Methylene Blue

Shomaila Khanam* & Sanjeeb Kumar Rout

Department of Physics, Birla Institute of Technology, Mesra, Ranchi, Jharkhand-835 215, India

Received 14 March 2022; accepted 19 May 2022

Bi_2WO_6 photocatalysts were synthesized via hydrothermal process and solid-state reaction techniques. The results revealed that Bi_2WO_6 prepared via hydrothermal route were composed of numerous square nanoplates, and Bi_2WO_6 prepared via solid-state route were just irregular broken pieces of the material. The photocatalytic activity of both the Bi_2WO_6 samples prepared via two different techniques under Xe lamp of 300W was evaluated for degradation Rhodamine B (RHB) and Methylene blue (MB). The hydrothermally prepared Bi_2WO_6 nanoplates exhibited better photocatalytic activity. Nearly 56% of RHB and 53% of MB were degraded within 40mins respectively, which was three times better than the Bi_2WO_6 synthesized by solid-state reaction. The better photocatalytic performance can be credited to the geometry, porosity, and the higher surface area of the hydrothermally prepared Bi_2WO_6 photocatalyst.

Keywords: Hydrothermal; Photocatalytic test; Degradation; Scavenger; Rhodamine B; Methylene blue

1 Introduction

The textile industries in recent times stand as a precarious problem in polluting water. About 15% of the dye is lost during the processing and is released directly into the water. The release of dye contaminated water is a substantial source of non-aesthetic pollution. Among all the most common dyes found in water bodies are rhodamine B (RHB) and methylene blue (MB) and is very hazardous to human as well as for water ecosystem. The degradation of these dyes with different photocatalysts has been an important research since a long time.

There are various literatures that have reported the degradation of dyes with different photocatalyst and different synthesis technique. Kian for *et al.* reported the photo catalytic degradation of RHB and MB up to 38.8% and 33.6% in 120 min under visible light irradiation over bare TiO_2 prepared by hydrothermal method[1]. In a recent literature by Khan *et al*. RHB and MB was degraded up to 62% and 71% in 240 min the presence of hydrothermaly prepared MoS_2 photocatalyst under UV irradiation[2]. Kumaran and team in 2019 reported the photo catalytic degradation of 7% of RHB by ZnO and 40% degradation of RHB in 25 min by CuO photacalysts prepared via solid-state reaction method[3]. Obregon *et al*. reported 66% and 43% degradation of RHB and MB in 180 mins over $BiVO_4$ photocatalyst[4].

In recent years, Bi_2WO_6, with a layered crystal structure, has proved to be a perfect visible light photocatalyst. There have been various methods, such as solid-state, sol-gel, solvothermal, and hydrothermal, utilized to synthesize Bi_2WO_6 for the evaluation of visible photocatalytic activities[5-8]. The preparation of photocatalyst plays an important role in defining the photocatalytic properties of materials. The synthesis techniques are expected to modify the structural and morphological characteristics of the material. The specified architectures exhibit unique physical and chemical properties depending on the size, shape, orientation, alignment, and dimensionality. As the photocatalytic activity totally correlates itself to the size, geometry, and morphology of the photocatalyst[9,10].

Solid-state synthesis of Bi_2WO_6 produces the photocatalyst in bulk and is economical but lacks in achieving desirable efficiency. The hydrothermal technique was first employed by Huang *et al*. & Xie *et al*. to prepare Bi_2WO_6 flake-ball particles in the presence of polyvinyl pyrrolidone (PVP) as a structure-directing agent[8,11]. Hydrothermal preparation is one of the optimum techniques for anisotropic crystal growth Bi_2WO_6 since the preparation conditions, such as temperature, pressure, the composition of the precursor, and the addition of a template, are easily tunable[12-14]. An increase in symmetry and crystallinity

*Corresponding author:
(Email: shomaila27t@gmail.com)

in the nanostructural photocatalysts enhances the photon absorption power, enhances charge separation, and improves the surface reaction.

Crystallites of Bi_2WO_6 possess Aurivillius phases and have the potential for photocatalytic decomposition of organic pollutants under visible light irradiation[9,15,16]. The crystal of Bi_2WO_6 consists of layers of WO_6 octahedral sheets at the corners and bismuth oxide sheets. It has been reported that a hydrothermally prepared Bi_2WO_6 undergoes anisotropic crystal growth and forms rectangle-shaped nanoplates[17,18].

In the present work, the comparative study of structural, morphological, and photocatalytic behavior of Bi_2WO_6 prepared via hydrothermally, and solid-state techniques has been done. The photocatalytic activities were evaluated by degrading toxic dyes like RhB and MB under visible light irradiation. It was found that the Bi_2WO_6 with nanoplates structure show the highest level of photocatalytic activity among Bi_2WO_6 samples with irregular morphology. Other structural, morphological surface, and optical characterizations were performed to elucidate the properties influencing the photocatalytic activity of Bi_2WO_6.

2 Experimental

2.1 Solid-state synthesis of Bi_2WO_6

In the cost-effective solid-state reaction technique for the synthesis of Bi_2WO_6 ceramics, the stoichiometrically calculated Bi_2O_3 (Sigma Aldrich, 99.99%) and WO_3 (Sigma Aldrich, 99.9%) were grounded in an agate mortar for 8h in a wet medium. The sample obtained was then calcined at 900 °C for 5h. The calcined powder mixture was then ground and was sent for phase purity characterization using an X-ray diffractometer.

2.2 Hydrothermal synthesis of Bi_2WO_6

In a typical hydrothermal procedure, 1.23g of $Na_2WO_4{\cdot}2H_2O$ and 3.64g of $Bi(NO_3)_3{\cdot}5H_2O$ were added to a Teflon vessel containing 150ml de-ionized water under magnetically stirring. The Teflon vessel was sealed in an autoclave, heated, and the temperature was set at 160 ºC for 20h. After the specified time of the reaction, the autoclave was allowed to cool down naturally to room temperature; the sample was centrifuged and washed several time with de-ionized water and then dried in an oven at 80 ºC for 10h. Finally, the yellowish powder of Bi_2WO_6 was obtained. Fig. 1 (a) shows the

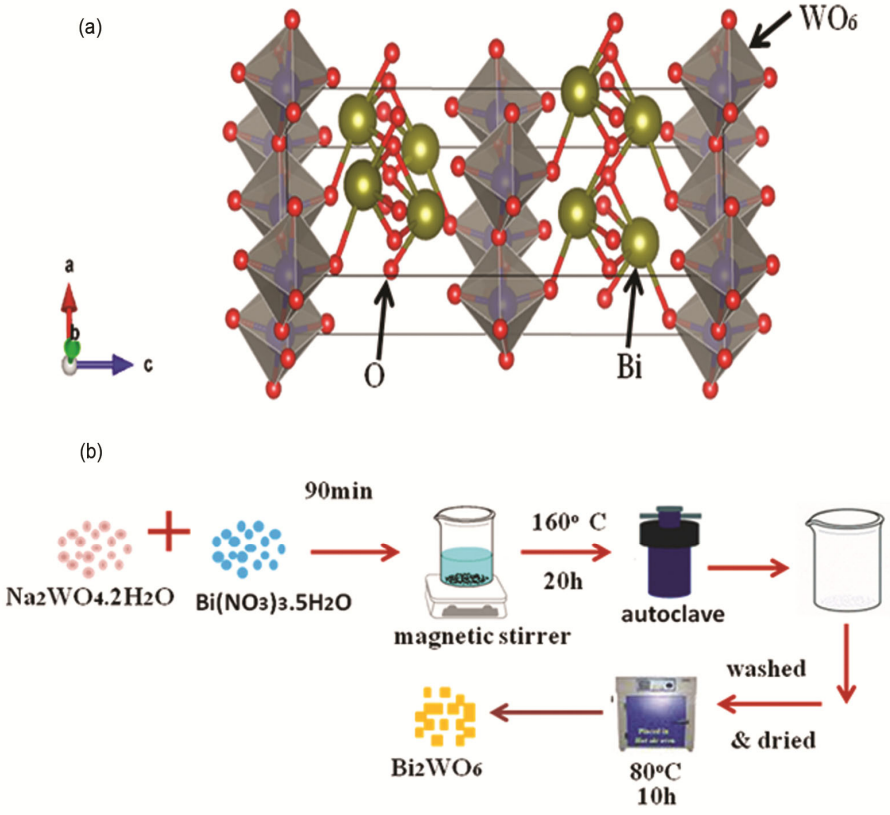

Fig. 1 — (a) crystal structure of Bi_2WO_6 and (b) Step for hydrothermal synthesis of Bi_2WO_6.

crystal structure of Bi_2WO_6 and Fig. 1(b) shows the pictorial representation of the hydrothermal synthesis of Bi_2WO_6.

2.3. Characterization

Phase purity was examined by x-ray diffraction (XRD) patterns using a Smart lab Rigaku, japan, diffractometer. The scanning rate was maintained to be $3°m^{-1}$, and the patterns were recorded in the 2θ range of 10^o–70^o using Cu Kα radiation (λ = 1.5416 Å). The detailed structural analysis was further analyzed using FTIR and Raman spectroscopy. FTIR spectra were recorded using Shimadzu Corpn., Japan, IR-Prestige 21 in the frequency range 400 to $4{,}000cm^{-1}$ using KBr, as a diluting agent. Raman spectra were examined by Reishaw UK Raman instrument. Morphological images were captured by using FESEM (ZEISS SIGMA 300) equipped with an energy dispersive x-ray spectroscope. The Brunauer-Emmett-Teller (BET) test was performed to analyze the surface area, pore-volume, and pore size distribution using Nova touch-LX1, Quantachrome. The prepared sample was degassed at 200°C for 4h prior to nitrogen adsorption-desorption measurement. The optical properties were recorded using a Perkin Elmer, USA; Lambda-25 UV-vis spectrometer in the range 200 to 800nm and a photoluminescence spectra by a Shimadzu, Japan, RF-5301 PC spectrofluorometer with an excitation wavelength of 360nm.

2.4 Photocatalytic experiment

The photocatalytic activity was examined by monitoring the degradation rate of dyes (RHB and MB). The test was performed in a photoreactor, and visible light irradiation was focused on it from the top. The degradation efficiency of the Bi_2WO_6 prepared via hydrothermal and solid-state methods was recorded after every ten minutes of the reaction. The photocatalytic degradation rate was calculated from the absorbance plot obtained via Ultraviolet and visible spectrometer. Photocatalytic experiment, was performed using 100ml of dye in water solution prepared from 10ppm of dye solution in de-ionized water was taken in a quartz glass beaker which allowed the penetration of light through it. And 20 mg of each photocatalyst was added to the dye solution. The dye-catalyst mixture was continuously stirred for 1h using a magnetic stirrer in dark conditions to allow the perfect adsorption of dye molecules on the photocatalyst's surface. The rotation speed of the magnetic stirrer was set at 700 rpm, and Xenon lamp of 300W attached with UV cut-off filter was maintained at a distance of 13cm from the photoreactor. After every ten minutes, 3 to 5 ml of aliquots were taken out and centrifuged and monitored under UV-vis spectrometer. The scavenger test was performed on the dye using the best performing prepared photocatalyst. $NaHCO_3$, IPA, and methanol were employed as a hole, OH*, and electron scavenger in order to know the active species participating in the photocatalytic reaction.

3 Results and discussion

3.1 Structural study

Figure 2 (a & b) shows the x-ray diffraction pattern of bismuth tungstate powder obtained by the hydrothermal method and the solid-state reaction method. The x-ray diffractogram of both the prepared sample shows the orthorhombic symmetry and matches completely with the JCPDS card no-79-2381. Both the diffractogram maintains the monophasic

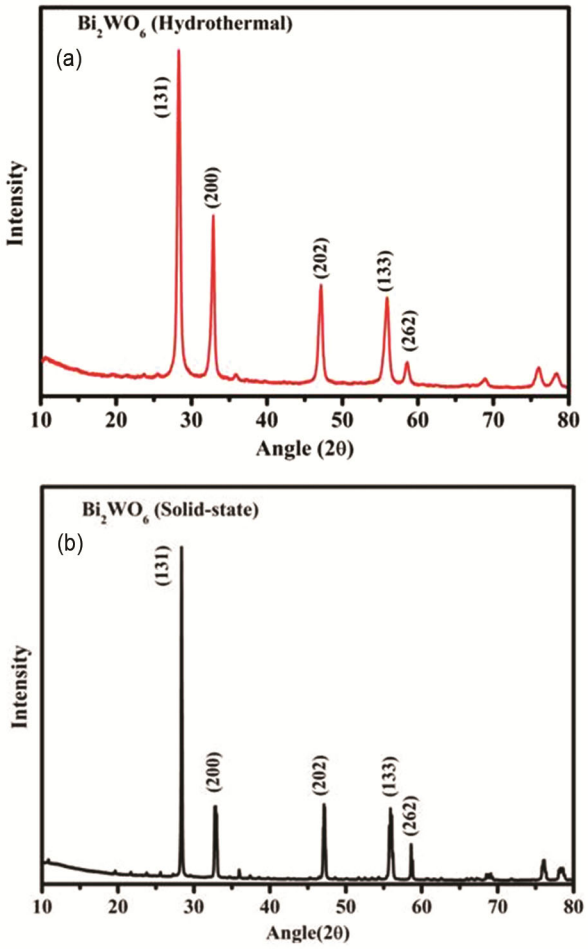

Fig. 2 — (a) X-ray diffractogram of hydrothermally prepared Bi_2WO_6 (b) and Bi_2WO_6 prepared via solid-state technique.

nature of Bi_2WO_6. The diffraction peaks in the case of hydrothermal synthesis are broader as compared to the corresponding peaks of solid-state synthesized Bi_2WO_6 sample, suggesting formation of fine grained (lower crystallite size) ceramics/powder in the hydrothermal reaction method. The average crystallite size of Bi_2WO_6 prepared by solid state reaction method was calculated to be 94.64 nm but hydrothermal technique reduced the crystallite size to 24.69 nm as calculated by Scherrer's formula.

Figure 3 shows the FESEM pictures of Bi_2WO_6 prepared via (a) solid-state and (b) hydrothermal procedure. FESEM image of solid-state synthesized Bi_2WO_6 in Fig. 3(a) does not present the formation of any crystalline structure whereas; Fig. 3(b) shows the numerous square nanosheets. The circular colonies of various nanosheets of diameter 200nm could be observed in Fig. 3(b). These nanosheets self assemble themselves in the form of circular colonies. The pores and the crystallinity of the observed nanosheet favours the adsorption of organic compounds and transfer of active species[9,19,20].

Figure 4(a) shows the FTIR spectra of Bi_2WO_6 prepared by solid-state and hydrothermal synthesis. Both the FTIR spectrum show absorption bands between frequency range 400 to 1000 cm-1, assigned to Bi-O stretching, W-O stretching, and W-O-W bridging stretching modes. The absorption bands at 501cm^{-1} and 709.5cm^{-1} is assigned to Bi-O and W-O stretching bond, respectively[21-23]. The unaltered band positions suggest no change in crystal symmetry during these synthesis techniques.

The experimental Raman spectra of Bi_2WO_6 with characteristic peaks in the wavenumber range of 200

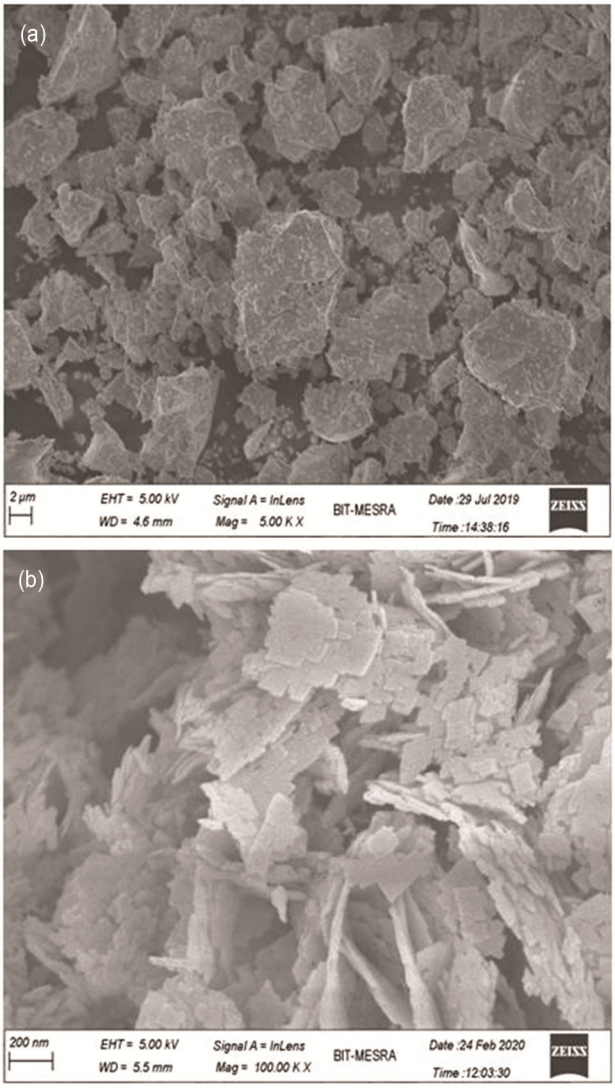

Fig. 3 — FESEM images of Bi_2WO_6 (a)hydrothermally prepared and (b) solid state reaction method.

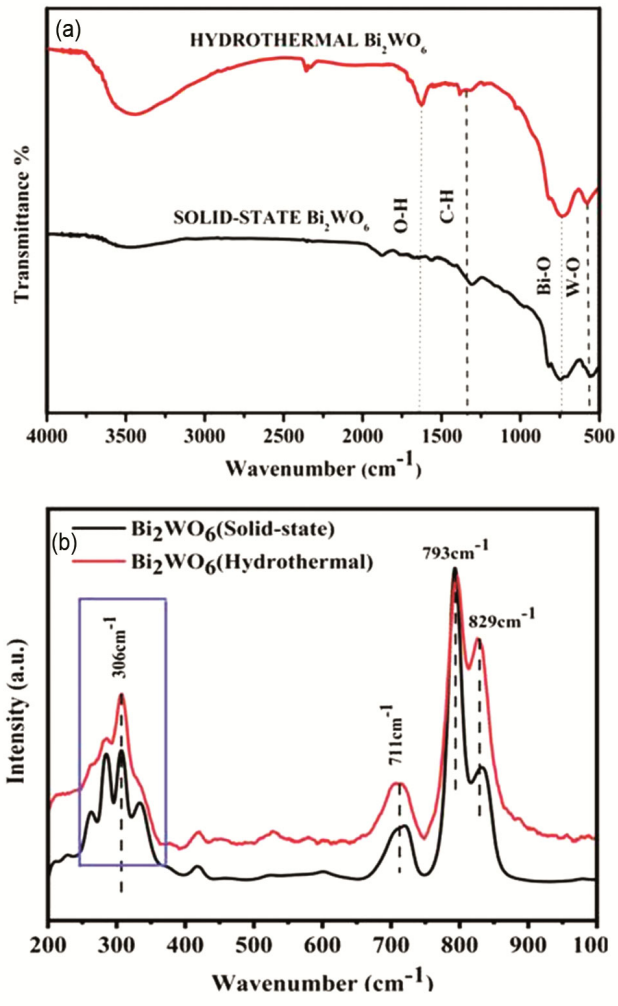

Fig. 4 — (a) FTIR and (b) Raman spectra of Bi_2WO_6 (H) and Bi_2WO_6 (S).

to 1000 cm^{-1}[24] at room temperature are shown in Fig. 4(b). The spectra of B_2WO_6 prepared by hydrothermal and solid-state technique showcase a similar profile. Sharp and well resolved Raman spectra of solid state synthesized Bi_2WO_6 suggests formation of crystalline and large grained catalyst. The peaks obtained in both the prepared sample are located at the same wavenumber, pointing at the same structural phase in spite of changing the synthesis method. The active modes at 792.94 cm^{-1} and 828.58 cm^{-1} may be assigned to the symmetric and antisymmetric modes of the O-W-O bonds[25]. The vibration at 334.46 cm^{-1} and 721.83 cm^{-1} are allocated to WO_2 mode[26,27] and linking mode of tungstates[28,29]. The peak at 307.23 cm^{-1} is due to the simultaneous translational motion of Bi^{3+} and WO_6^{6-} [25]. However, the position of all Raman peaks in the Raman spectra of both the samples did not change and goes well with the orthogonal Bi_2WO_6. The similar Raman spectra indicates that the change in synthesis technique did not change the crystal growth direction of Bi_2WO_6, but may change the size, surface area, porosity and geometry of the grain.

Figure 5 shows the N_2 adsorption-desorption isotherm, and the corresponding pore size distribution (inset) of the prepared photocatalysts prepared via hydrothermal and solid-state technique. The specific surface area of Bi_2WO_6 and pore volume of Bi_2WO_6 prepared hydrothermally was calculated to be 26.4095 m^2/g *and 0.1294 cc/g, respectively. Whereas the surface area and pore volume of* Bi_2WO_6 *prepared via solid-state technique were calculated to be 2.8700* m^2/g *and 0.008cc/g, respectively.* The BJH pore size distribution plot of hydrothermally prepared Bi_2WO_6 shows a narrow range of pore size distribution with an average pore diameter of 14nm, indicating the mesoporous characteristic of the photocatalyst. But in the case of Bi_2WO_6 prepared through solid-state technique, the average pore diameter was observed to be 3.6nm, representing less porosity in the material. Thus, the hydrothermal Bi_2WO_6 shows a substantial increase in pore size, volume, and surface area as compared to the solid-state Bi_2WO_6.

3.2 Optical study

The optical band gap was calculated by using the equation of Kubelka-Munk and is shown in Fig. 6(a). The inset plot shows the absorbance graph of the prepared sample. The intensity of the absorbance plot of hydrothermally prepared Bi_2WO_6 is lower than the Bi_2WO_6 prepared via solid-state technique. The optical bandgap of the two samples was calculated from the equation (1) given below.

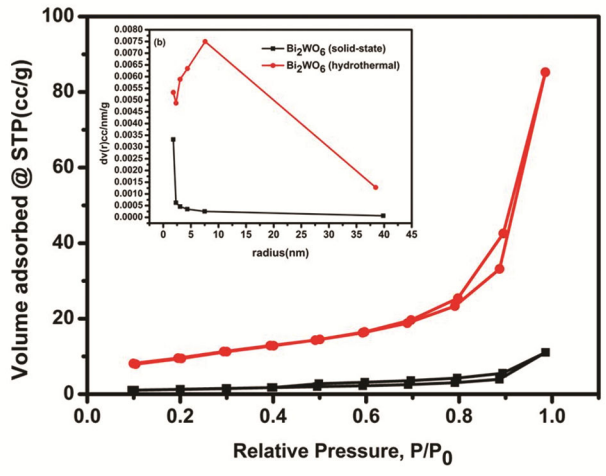

Fig. 5 — N_2 adsorption-desorption isotherm inset shows pore size distribution of Bi_2WO_6 (H) and Bi_2WO_6 (S).

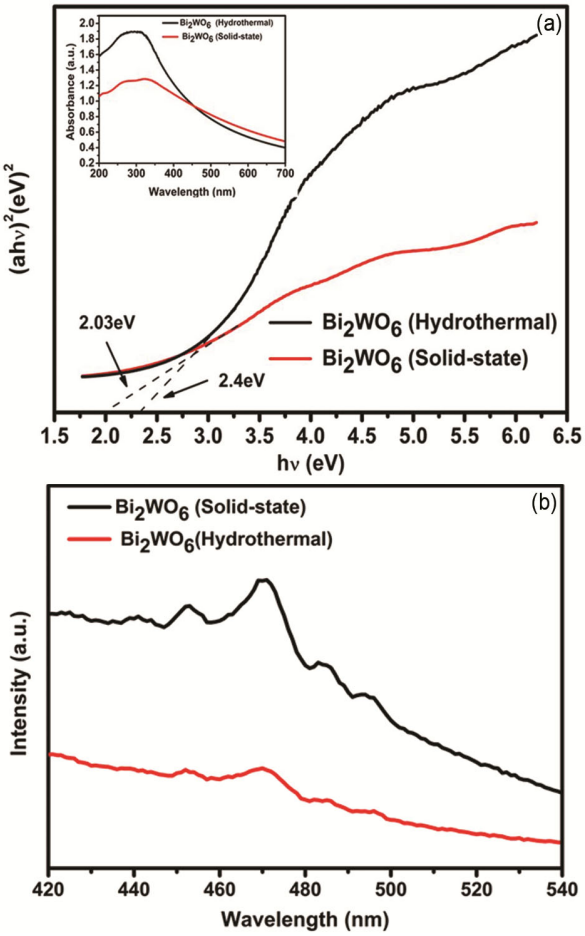

Fig. 6 — (a) tauc plot and the inset shows absorbance graph (b) PL spectra of Bi_2WO_6 (H) and Bi_2WO_6 (S)

$$[F(R)\,h\nu]^{1/n} = C_1\,(E_{gap} - h\nu) \quad ...(1)$$

Here F(R) is the Kubelka-Munk function, $h\nu$ is the energy, and C_1 is the constant[30]. The optical energy band gap of the Bi_2WO_6 prepared via solid-state and hydrothermal, determined by tauc plot was found to be 2.4eV and 2.03ev, respectively.

Figure 6(b) represents photoluminescence (PL) emission spectra of hydrothermally and solid-state synthesized Bi_2WO_6. Photoluminescence serves well in providing us the knowledge of the recombination rate of photoexcited charge carriers. The weaker PL intensity of hydrothermally prepared Bi_2WO_6 indicates a lower recombination rate of photogenerated electron-hole pairs[31], and higher PL intensity of the Bi_2WO_6 prepared by solid-state technique describes its higher recombination rate of photo charge carriers. The PL result goes well with the photocatalytic result, and hydrothermally prepared Bi_2WO_6 proves to be a better photocatalyst.

3.3 Degradation of RHB and MB

The photocatalytic activity of Bi_2WO_6 prepared by two different techniques was performed by degrading RHB and MB under visible light irradiation. RHB and MB has maximum absorption at 554 nm and 664nm. RHB and MB get more easily adsorbed by hydrothermally prepared Bi_2WO_6 catalyst than by Bi_2WO_6 catalyst prepared by solid-state illustrated in Fig. 7(a), (b), and 8(a), and (b). The higher removal efficiency has been observed in a hydrothermally prepared photocatalyst. This is totally contributed to the morphology of the obtained crystal. The FESEM images of Bi_2WO_6 prepared via hydrothermal technique shows more crystalline flakes and nanosheets structure, whereas the FESEM images of Bi_2WO_6 prepared via solid-state procedure appeared just as broken pieces of rock; The BET result also showed that the synthesis technique had changed the surface area of Bi_2WO_6. The higher surface area, reduced size and crystalline geometry enhanced the photoactivity of hydrothermally prepared catalysts. Higher surface area and lower size of the catalysts adsorbs more dye molecules and increases the active sites for the reaction while the geometry reduces the recombination rate of electron-hole pair generated, thus enhances the photocatalytic degradation of RHB and MB dyes.

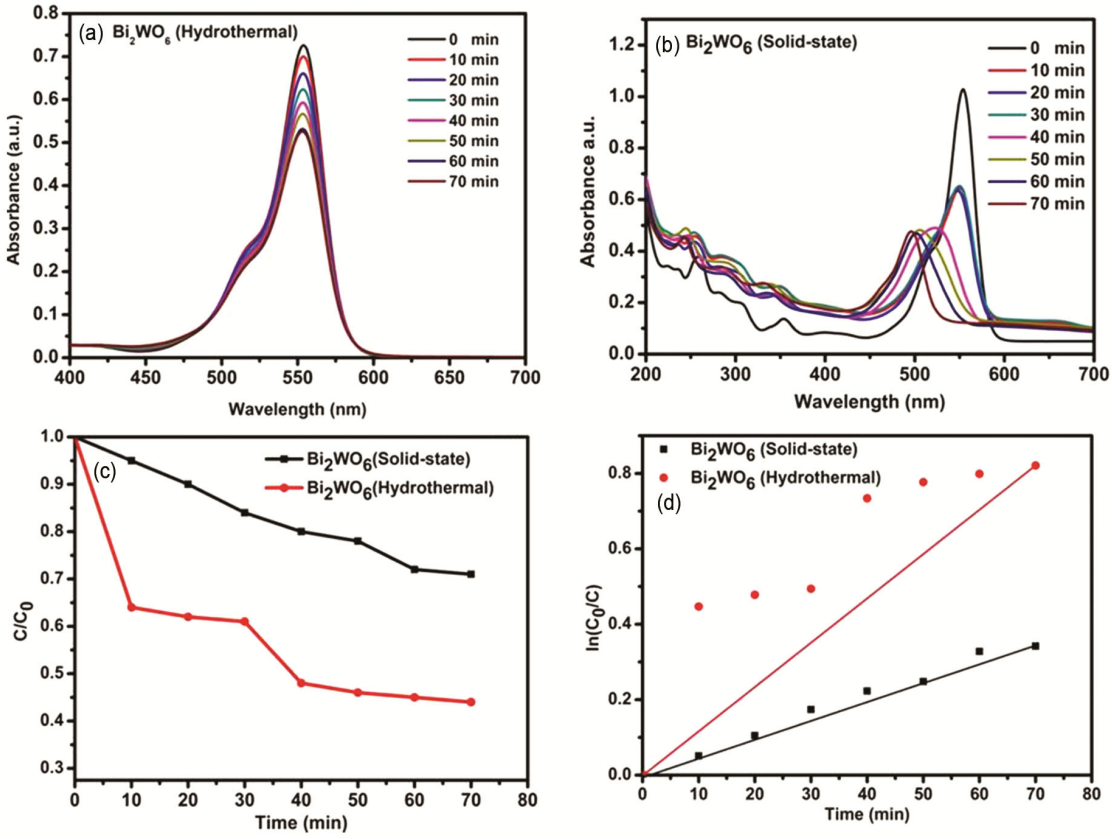

Fig. 7 — The photocatalytic activity of (a) RHB in the presence of Bi_2WO_6 (S) and (b) Bi_2WO_6 (H) (c) degradation efficiency of Bi_2WO_6 (S) and Bi_2WO_6 (H) (d) first order reaction rate constant.

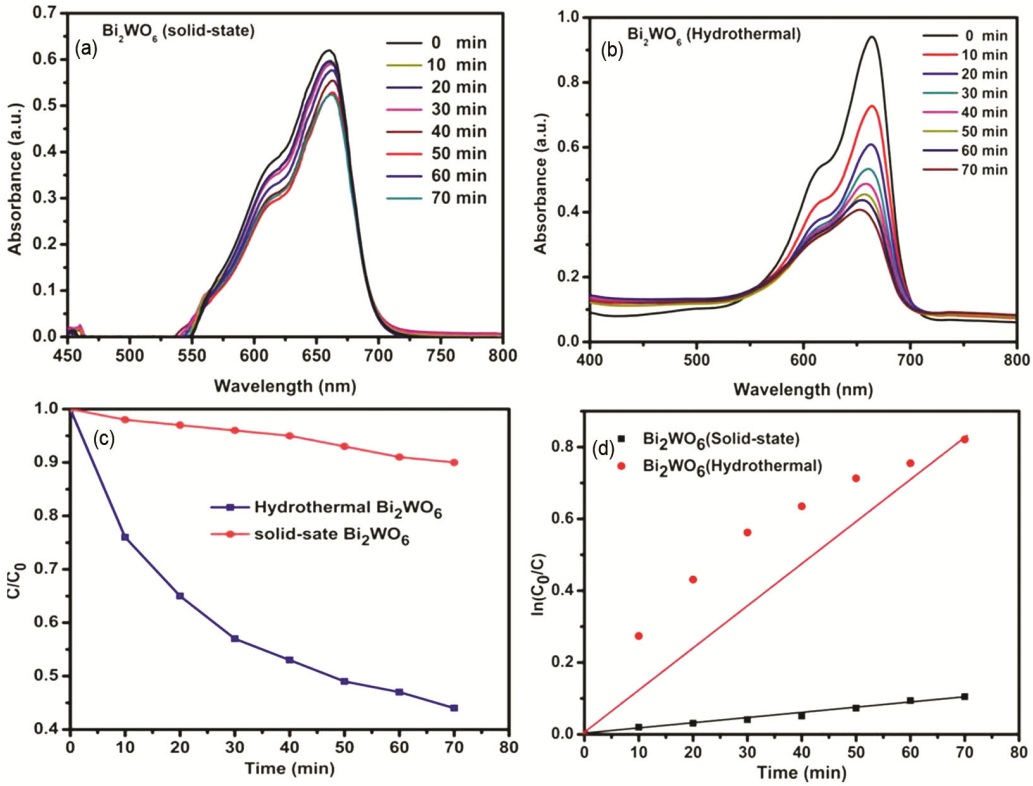

Fig. 8 — The photocatalytic activity of (a) MB in the presence of Bi_2WO_6 (S) and (b) Bi_2WO_6 (H) (c) degradation efficiency of Bi_2WO_6 (S) and (b) Bi_2WO_6 (H)) (d) first order reaction rate constant.

Hydrothermally prepared Bi_2WO_6 shows much better performance and degrades up to 56% and 53% of RHB and MB in 70mins respectively. In comparison, the Bi_2WO_6 prepared by solid-state technique degraded only 20% and 16% of RHB and MB respectively. The aliquots of the dye were monitored after every ten minutes by UV spectrometer, and it was observed that the absorption peak of RHB at about 554 nm decreases gradually with time and under visible light irradiation and is followed by the absorption band shift from 554 nm to 498 nm. The blue shift of the absorption peak is due to the de-ethylation process[28] (Fig. 9(a)) which occurs as the light irradiation time increases. The breakdown pathway of RHB includes: RHB at 554 nm forms N,N,N′-Triethyl-rhodamine at 539 nm, N.N′-Diethyl-rhodamine at 522 nm; N-Ethyl-rhodamine at 510 nm; and ultimately to Rh-110 at wavelength 498 nm[32]. The intermediate products from degradation of MB is azure A, azure B azure C and thionin that is formed *via* demethylation cleavage during the photocatalytic degradation (Fig. 9(b))[33].

Figure 7 (c) & 8 (c) represents the change in the relative concentration of RHB and MB over Bi_2WO_6 prepared via hydrothermal and solid-state technique as a function of irradiation time. Fig. 7(d) & 8(d) shows the kinetic plot of an apparent first order rate constant (k_{app}) which was calculated from the equation (2).

$$\ln(C_0/C)=K_{app}t \quad ...(2)$$

Bi_2WO_6 hydrothermally prepared and Bi_2WO_6 prepared via solid state nanocomposites exhibited apparent rate constants of respectively, showing that Bi_2WO_6 prepared via hydrothermal reaction enhanced the photocatalytic activity.

3.4 Photocatalytic stability

Experiments were performed to test the photocatalytic stability of the Bi_2WO_6 prepared via hydrothermal technique. It was observed that the photocatalytic degradation efficiency of the catalyst demonstrated at the same temperature and irradiation time on RHB, was maintained for the next five cycles (Fig. 10(c)) only a slight decrease after every cycle was noticed that might be due to aggregation of the nanocomposites. FT-IR spectra of hydrothermally prepared Bi_2WO_6 nanocomposite before and after the

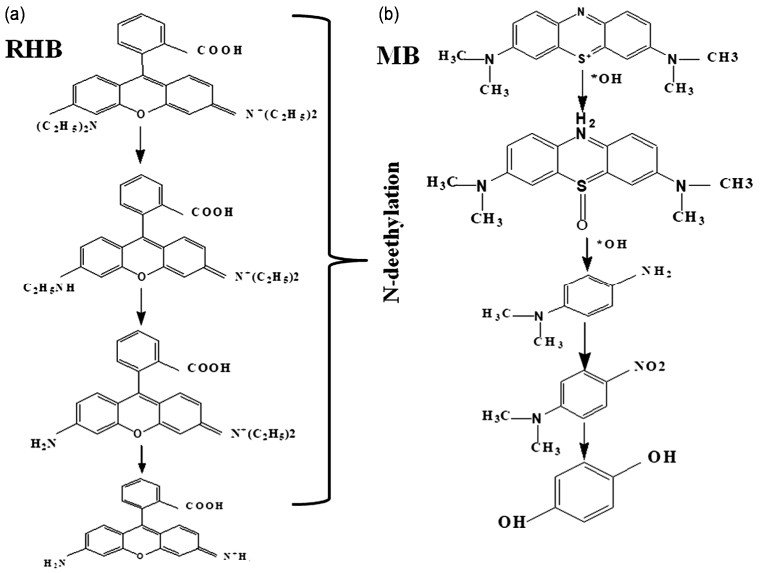

Fig. 9 — Photodegradation pathway of (a) RHB and (b) MB

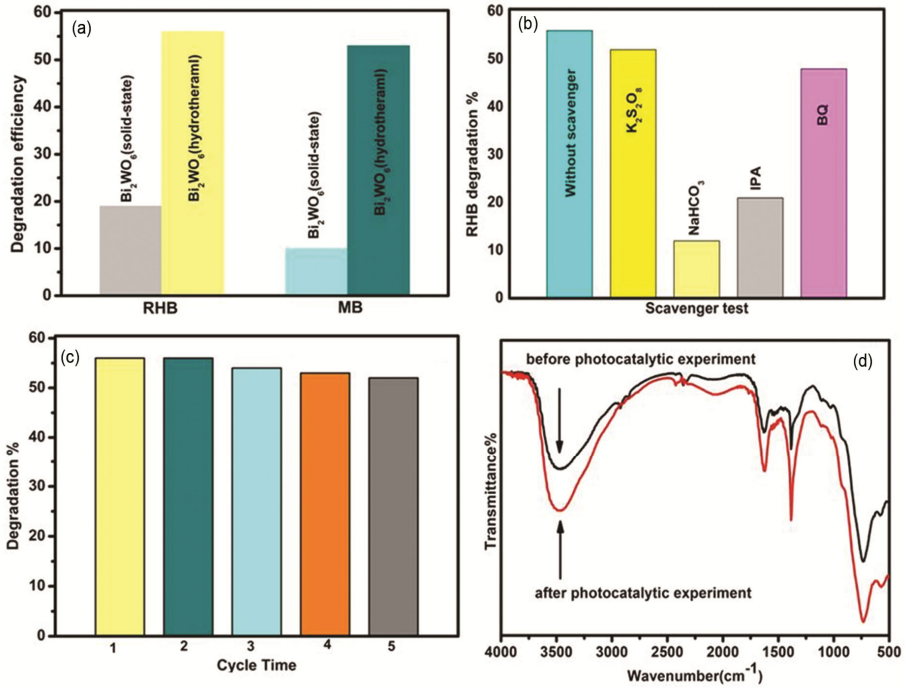

Fig. 10 — (a) Degradation effeciency of the prepared photocatalyst (b) scavenger test result employing $NaHCO_3$, IPA, and methanol and(c) reusibility

photocatalytic reaction were used to explain the stability of the nanocomposite (Fig. 10d). The shapes of the FT-IR spectra before and after photocatalysis exhibited similar profile, thus showing no change in the chemical structure of the catalyst. The hydrothermally prepared Bi_2WO_6 shows a good stability can be reused efficiently.

3.5 Scavenger test

The scavenger test can give the best and absolute result of the species active in the photocatalytic reaction. For the scavenger test, $NaHCO_3$ (20mg), IPA ($0.01 molL^{-1}$), $K_2S_2O_8$ and Benzoquinine (BQ) ($0.01 molL^{-1}$) were employed as an h^+, OH*, e^- and $.O_2$ scavenger, respectively. The experiment was similar

to the photocatalytic test; only the scavengers were incorporated into the reaction. Fig. 10(a) shows the degradation efficiency of the prepared photocatalyst over RHB and MB dye which is calculated from the equation (3).

$$n = \frac{C_0 - C}{C_0} * 100 \quad ...(3)$$

and Fig. 10 (b) shows the effect of scavengers in degradation efficiency of the photocatalyst over RHB. The addition of $NaHCO_3$ and IPA reduced the degradation of RHB to 12% and 21% respectively, thus depicting the dominant role of holes in the degradation of dyes. The addition electron scavenger and superoxide scavenger does not show many changes in the degradation efficiency of the photocatalyst depicting the dormant role of e^- and $.O_2$ in the reaction.

4 Photocatalytic mechanism

The photo catalytic mechanism of Bi_2WO_6 can be explained by the reactions shown in equation (4), (5), (6) and (7).

$$Bi_2WO_6 + h\nu \rightarrow Bi_2WO_6\ (e^- + h^+) \quad ...(4)$$

$$e^- + O_2 \rightarrow {}^{\cdot}O_2^- \quad ...(5)$$

$$h^+ + H_2O/OH^- \rightarrow {}^{\cdot}OH \quad ...(6)$$

$$MB + ROS \rightarrow CO_2 + H_2O \quad ...(7)$$

To explore the detailed mechanism we the knowledge of the potential band is useful. The conduction band and the valence band potential can give us an idea of the generation and action of charge pairs. The Mullikans equation[34] can help in calculating the conduction and valence band potential and is written as equation (8).

$$E_{CB} = X - E_c - \frac{E_g}{2} \quad ...(8)$$

Here X is the arithmetic mean of electron affinity and ionization potential of the catalyst and is calculated to be 7.26 eV. The E_c is the kinetic energy of free electrons of the hydrogen scale (4.5eV), and E_g is the optical energy band gap of Bi_2WO_6 (hydrothermally prepared) was calculated to be 2.03eV[28]. The conduction band and valence band potential of hydrothermally Bi_2WO_6 versus normal hydrogen electrode was calculated to be 1.75 eV and 3.78 eV.

In general, the photocatalyst absorbs light energy ($h\nu$) when irradiated by visible light and excites the electrons from the VB to the CB, thus creating e^- in the conduction band and h^+ in the valence band. The photogenerated e^- and h^+ migrate to the surface of the photocatalyst and contribute to a photocatalytic reaction, and decomposes the organic pollutant in solution. Fig. 11 shows the pictorial representation of the photocatalytic reaction taking place between photocatalyst and dye solution.

According to the thermodynamics, the amount of O_2^- produced in the reaction should be very less than

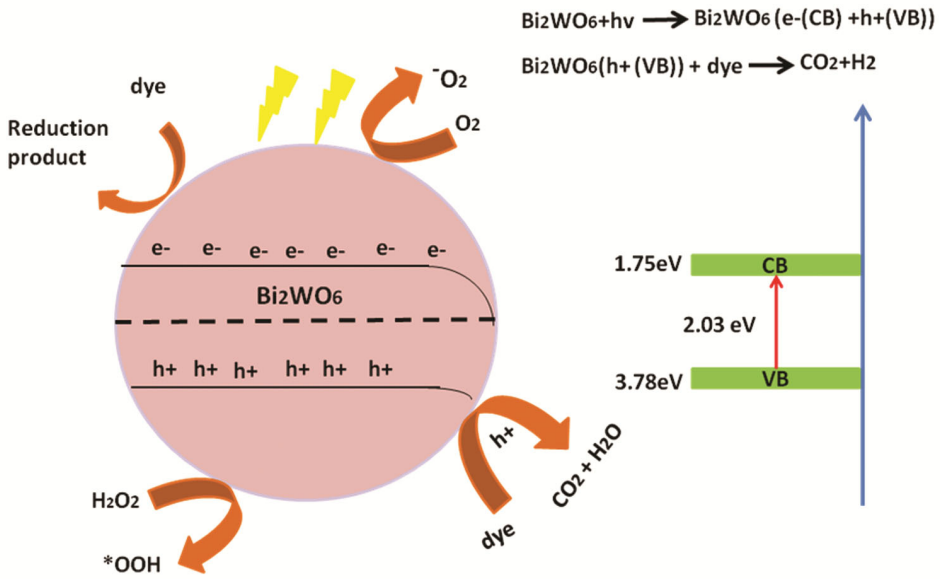

Fig. 11 — Schematic diagram of the photocatalytic reaction taking place between photocatalyst and dye solution.

that of ·OH, since E_{CB} of Bi_2WO_6 (H) was about 1.75 eV, which is very much positive than $O_2/*O_2^-$ (−0.33 eV *vs.* NHE)[35,36]. And the E_{VB} of Bi_2WO_6 (H) was calculated to be 3.78 eV, which is more positive than the potential of $OH^-/·OH$ (2.38 V *vs.* NHE) and $H_2O/·OH$ (2.72 V *vs.* NHE). The thermodynamic result shows that the photoexcited h^+ can readily react with OH^- and H_2O to produce *OH radicals which participate in the reaction.

5 Conclusion

The Bi_2WO_6 photocatalysts were successfully synthesized by hydrothermal and solid-state methods. The phase and the structural study obtained by XRD, FT-IR, and Raman do not show any changes in the profile of the prepared samples. But the XRD peaks broadened as the synthesis technique changed from solid-state to hydrothermal. The optical study showed higher light absorption capability and lower electron-hole recombination in the case of Bi_2WO_6 prepared via hydrothermal technique. The morphology of hydrothermally Bi_2WO_6 observed in FESEM represents crystallite nanosheets, whereas Bi_2WO_6 synthesized by solid-state method showed irregular pieces. The optical and morphological result goes well with the photocatalytic test result. Hydrothermally prepared Bi_2WO_6 was three times better than Bi_2WO_6 prepared via the solid-state procedure in degrading RHB and MB. The scavenger test demonstrated that h^+ was the active species and participated in the photocatalytic degradation of the dyes in the presence of photocatalyst.

Acknowledgement

This work was financially supported by the Department of Science and Technology, Govt. of India, under the WOS-A scheme (SR/WOS-A/CS-128/2018).

Conflict of interests

The authors declare no conflict of any kind of interest.

References

1 Xu X, Zhou X, Zhang L, Xu L, Ma L & Luo J, *Mater Res Bull,*70 (2015) 106.
2 Khan M I, Hasan M S, Bhatti K A, Rizvi H, Wahab A & Rehman S U, *Mater Res Express,* 7 (2020) 015061.
3 Kumaresan N, Sinthiya M M A, Ramamurthi K, Babu R R, & Sethuraman K, *Arab J Chem,* 13 (2020) 3910.
4 Obregón S & Colón G, *J Mol Catal A Chem, 376 (2013)* 40.
5 Ma D, Huang S, Chen W, Hu S, Shi F & Fan K *J Phys Chem C,* 113 (2009) 4369.
6 Lee W L W, Huang S T, Chang J L, Chen J Y, Cheng M C & Chen C C, *J Mol Catal A Chem* 361 (2012) 80 .
7 Liu Y, Wang W, Fu Z, Wang H, Wang Y & Zhang J, *Mater Sci Eng, B* 176 (2011) 1264.
8 Zhang Z, Wang W, Shang M & Yin W, *J Hazard Mater,* 177 (2010) 1013.
9 Hoffmann M R, Martin S T, Choi W & Bahnemann D W, *Chem Rev,* 95 (1995) 69.
10 Zhang L, Wang H, Chen Z, Wong P K & Liu J, *Appl Catal B,* 106 (2011) 1.
11 Zhang G, Lü F, Li M, Yang J, Zhang X & Huang B, *J Phys Chem Solids,* 71 (2010) 579.
12 Amano F, Nogami K, Abe R & Ohtani B, *J Phys Chem C,* 112 (2008) 9320.
13 Yu S H, Liu B, Mo M S, Huang J H, Liu X M & Qian Y T, *Adv Funct Mater,* 13 (2003) 639.
14 Xu Y, Chen D & Jiao X, *J Phys Chem,* 109 (2005) 13561.
15 Tang J, Zou Z & Ye J, *Catal Letters,* 92 (2004) 53.
16 Shimodaira Y, Kato H, Kobayashi H & Kudo A, *J Phys Chem,* 110 (2006) 17790.
17 Shen J, Xue J, Chen Z, Ni J, Tang B & He G, *J Mater Sci,* 53 (2018) 4848.
18 Fu H, Zhang L, Yao W & Zhu Y, *Appl Catal,* 66 (2006) 100.
19 Zhang L, Wang W, Chen Z, Zhou L, Xu H & Zhu W, *J Mater Chem,* 17 (2007) 2526.
20 Wu Q S, Cui Y, Yang L M, Zhang G Y & Gao D Z, *Sep Purif Technol,* 142 (2015) 168.
21 Yu J, Xiong J, Cheng, B, Yu Y & Wang J, *J Solid State Chem,* 17 (2005) 1968.
22 Xia J, Li H, Luo Z, Xu H, Wang K & Yin S, *Mater Chem Phys,* 121 (2010) 6.
23 Bunluesak T, Phuruangrat A & Thongtem S, *Res Chem Intermed,* 47 (2021) 3079.
24 Nobre F X, Junior W A G P, Ruiz Y L, Bentes V L I, Silva-Moraes M O, Silva T M C & Brito W R, *Mater Res Bull,* 109 (2019) 60.
25 Maczka M, Hanuza J, Paraguassu W, Gomes Souza Filho A, Tarso Cavalcante Freire P & Mendes Filho J, *Appl Phys Lett,* 92 (2008) 112911.
26 Kania A, Niewiadomski A & Kugel G E, *Phase Transit,* 86 (2013) 290.
27 Mishra R K, Weibel M, Müller T, Heinz H, & Flatt R J, *Chimia Int J Chem,* 71 (2017) 451.
28 Fu H, Pan C, Yao W & Zhu, Y, *J Phys Chem,* 109 (2005) 22432.
29 Frost R L, Duong L & Weier M, *Spectrochimica Acta Part A: Molecular and Biomolecular Spectroscopy,* 60 (2004) 1853.
30 Hong J, Hu Z, Probert M, Li K, Lv D & Yang X, *Nat Commun,* 6 (2015) 1.
31 Fujihara K, Izumi S, Ohno T & Matsumura M, *J Photochem Photobiol,* 132 (2000) 99.
32 Watanabe T, Takizawa T & Honda K, *J Phys Chem A,* 81 (1977) 1845.
33 Yang C, Dong W, Cui G, Zhao Y, Shi X & Xia X, *RSC Adv*, 7 (2017) 23699.
34 Frese Jr K W, Madou M J & Morrison S R , *J Phys Chem , A* 84 (1980) 3172.
35 Huang C, Chen L, Li H, Mu Y & Yang Z, *RSC Adv*, 9 (2019) 27768.
36 Tian Y, Zhang L & Zhang J, *J Alloys Compd,* 537 (2012) 24